Understanding of large auxetic properties of iron-gallium and iron-aluminum alloys

Yan-ning Zhang,[1] Ru-qian Wu,[1,a)] Holly M. Schurter,[2] and Alison B. Flatau[2]
[1]*Department of Physics and Astronomy, University of California, Irvine, California 92697-4575, USA*
[2]*Department of Aerospace Engineering, University of Maryland, College Park, Maryland 20742, USA*

(Received 11 December 2009; accepted 10 May 2010; published online 28 July 2010)

Large auxetic properties of iron-gallium and iron-aluminum alloys have been investigated with both theoretical and experimental approaches. Tensile tests of single-crystal iron-gallium alloys with compositions of 12%–25% gallium were conducted to determine the composition dependent values of the Poisson's ratio. Systematic density functional calculations revealed a simple correlation between the Poisson's ratio and tetragonal shear modulus. We attribute the auxetic properties of these intermetallic alloys to the drastic reduction in C' with the presence of metalloid atoms in the DO_3-type structures. © *2010 American Institute of Physics*. [doi:10.1063/1.3445269]

I. INTRODUCTION

Auxetic materials exhibit transverse expansion when they are stretched, rather than contraction as expected for most materials. This special feature is very useful in applications such as strain amplifiers, packing materials, energy absorption components, and soundproofing materials.[1] Much of the recent interest in auxetic materials started with development of auxetic foams.[2] Highly negative Poisson's ratios, with values as low in magnitude as -12 in porous polytetrafluoroethylene,[3] can be found in various manmade materials, many of which are flexible and some of which have hingelike, re-entrant honeycomb, or nodule-fibril structures.[4] More recently, carbon nanotube (CNT) films or CNT/polymer composite were also found to be auxetic and a grid network model was proposed to explain auxetic behaviors.[5] Many elemental metals as well as some alloys and oxides exhibit auxeticity along certain crystallographic axes but Poisson's ratios in these materials are usually low in magnitude, ~ -0.1.[6,7] Baughman *et al.*[8] found a correlation between the work function and the extremal values of Poisson's ratio for some of these materials and interpreted it with an electron-gas model. Alderson *et al.* used rotation and dilation of molecular square/tetrahedral frameworks to explain the auxetic behavior of α-quartz and α-cristobalite.[9,10]

In this paper, we discuss the origin of the unusually large auxetic features of two structural, iron-based alloys: $Fe_{100-x}Ga_x$ and $Fe_{100-x}Al_x$, where $0<x\leq 35$, namely, Galfenol and Alfenol. Galfenol with $x=25$ has been reported to have a negative Poisson's ratio along the [110] crystallographic axis of $\nu(110,1\bar{1}0)=-0.7$.[11] These two alloys are believed to be the first of the class of structural auxetic alloys, i.e., of high-modulus, molecular auxetic materials (with $E_{[110]}=\sim 100$ GPa for $Fe_{75}Ga_{25}$). Both of these alloys also exhibit large tetragonal magnetostriction, up to 400 ppm in $Fe_{80}Ga_{20}$, under low saturating magnetic fields.[12–15] Being auxetic and magnetostrictive along with having excellent mechanical properties, such as ductility and high yield strength, suggests these materials as candidates for use as active structural auxetic materials in sensors and molecular sieves, applications for auxetic materials suggested by Alderson and Evans[10] among others. It is, therefore, important to understand the auxetic properties of these alloys for the benefit of both fundamental science and maximizing their potential for use in practical applications.

For cubic materials, the Poisson's ratio along the ⟨110⟩ crystallographic directions can be expressed as a function of elastic stiffness constants, C_{ij}

$$\nu(110,1\bar{1}0)=\frac{(C_{11}-C_{12})\dfrac{C_{11}+2C_{12}}{C_{11}}-2C_{44}}{(C_{11}-C_{12})\dfrac{C_{11}+2C_{12}}{C_{11}}+2C_{44}}=\frac{1-A\dfrac{C_{11}}{3B}}{1+A\dfrac{C_{11}}{3B}}. \quad (1)$$

Here $A=2C_{44}/(C_{11}-C_{12})$ denotes the anisotropy of elastic moduli against diagonal and tetragonal distortions and B is the bulk modulus. For stable cubic structures, the tetragonal shear modulus $C'=(C_{11}-C_{12})/2$ and hence A are both positive, and therefore the sign of the Poisson's ratio is solely determined by the numerator of Eq. (1). In particular, negative Poisson's ratios may occur when $A>3B/C_{11}$ or $C'<C_{44}(C_{11}/3B)$. This reflects the need for strong elastic anisotropy or substantially small bulk modulus as a requirement for a material to be auxetic.

In the following, we first discuss the experimental and theoretical procedures for the determination of elastic constants and Poisson's ratios of $Fe_{100-x}Ga_x$ and $Fe_{100-x}Al_x$. Density functional calculations satisfactorily reproduced measured mechanical properties of Galfenol and Alfenol, including their Poisson's ratios. Interestingly, the key factor for producing elastic anisotropy and, subsequently, the auxetic behavior of these alloys, is attributed to an unlikely distribution pattern of Ga and Al atoms within the Fe lattice, in which these atoms need to be far apart from each other.

a)Electronic mail: wur@uci.edu.

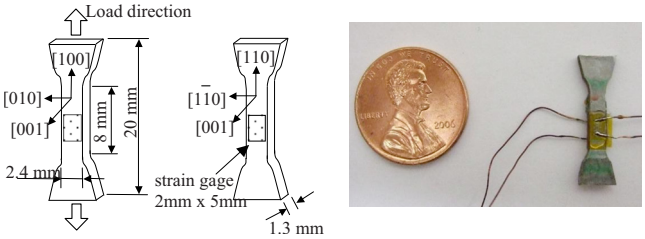

FIG. 1. (Color online) Schematic and photo of the [100] and [110] Fe–Ga dogbone tensile samples used in this study.

II. EXPERIMENTAL PROCEDURES

Single crystal $Fe_{100-x}Ga_x$ samples targeting $x=12.5$, 18.75 and 25 were synthesized at the Materials Preparation Center, Ames Laboratory[16] in an alumina crucible with the modified Bridgman technique, by arc-melting Fe (99.99% purity) and Ga (99.999% purity) several times under an argon atmosphere. The arc-melted button was then re-melted, and the alloy was drop-cast into a copper chill cast mold to ensure compositional homogeneity throughout the ingot. The alloy was heated in a vacuum of 1.3×10^{-4} Pa up to 1075 K to degas the crucible and charge. The chamber was then backfilled to a pressure of 275 kPa with high purity argon. The ingot was further heated to the growth temperature and held for one hour to allow thorough mixing before withdrawing the sample from the heat zone at a rate of 4 mm/h. Following growth, the ingot was annealed at 1000 °C for 168 h. The 18% samples were additionally annealed later for one hour at 800 °C under flowing argon and then water quenched.

The single crystal's orientation was determined within 0.25° using the Laue x-ray back-reflection and then cut into tensile specimens by electrodischarge machining. Several dog-bone shaped specimens were cut from each ingot, having the nominal dimensions indicated in Fig. 1. At least one sample from each ingot was aligned with the [100] crystallographic axis parallel to the load direction and one sample aligned with the [110] axis parallel to the load direction. After machining, the orientation of each specimen was again checked by the Laue x-ray back reflection. Energy dispersive x-ray spectroscopy (EDS) and wavelength dispersive x-ray spectroscopy were used to determine the composition of each specimen. A sample of known composition of $Fe_{35}Ga_{65}$ was used with each specimen as the calibration standard. Three points were chosen along the surface of each sample, and the composition at each point was measured to an accuracy of 0.21 percent or better.

An MTS Systems Corporation hydraulic load stand was used for tensile testing. Special alignment and gripping fixtures were used to accommodate the small size of the specimens and to ensure that the load was applied along the length of the samples. The gripping fixtures applied a normal stress to the wide facets of the dog-bones, and were connected to the MTS load stand at the base and moving cross arm with universal joints. Tests were conducted in constant cross-arm velocity mode at a nominal rate of either 0.5 or 1.0 μm/sec to a maximum tensile load of approximately 150 MPa, staying well below the elastic limit of ~500 MPa, and producing with similar results for both loading rates. Each specimen had two strain gauges attached to it, one on each side of the dog-bone gage section (see Fig. 1). One strain gauge measured strain in the longitudinal direction (Vishay Micro Measurements EA-06–015DJ 120) and the other measured the strain in the transverse direction (EA-06–015EH 120). Each sample was tested twice with a new set of strain gauges. Because of differences in cross-sectional area, the stress varied slightly for each sample. The tests were done at room temperature and zero magnetic field. A finite element model of the dog-bone tensile sample was generated using commercial software ANSYS to check the stress distribution induced throughout the sample as tensile loads were applied to the gripping fixtures. This model showed a uniformly constant stress throughout the region of the sample that was covered by strain gauges and throughout most of the narrow gage region of the dog-bone (i.e., except at the ends where the sample width starts to change).[17] We estimate that the electric current in the strain gauge circuit produces a magnetic field less than a few tenth millitorrs at the center and, therefore, has no significant effect on our measurements.

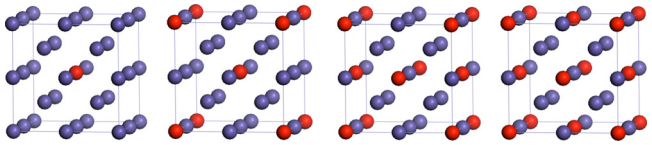

FIG. 2. (Color online) Atomic configurations for the cubic structures of $Fe_{100-x}Ga_x$ and $Fe_{100-x}Al_x$ alloys with $x=6.25$, 12.5, 18.75, and 25. Blue (dark grey) and red (grey) balls are for Fe and Ga/Al atoms, respectively.

III. DETAILS OF DENSITY FUNCTIONAL MODELING

We performed density functional calculations at the level of the generalized gradient approximation (GGA),[18] using the Vienna *ab initio* simulation package (VASP).[19] The projector augmented wave[20] potentials were adopted for the description of electron-ion interactions. For Ga, we treated the 3*d* shell in the valence band. It is well accepted that Ga and Al tend to avoid forming first neighborhoods in the bcc lattice of Fe. Our test calculations indicate that the presence of Ga–Ga or Al–Al first neighbors significantly increase total energies, by 0.1–0.3 eV per pair. Therefore, we used 16 atom cubic supercells without Ga–Ga (Al–Al) first neighbors as displayed in Fig. 2 for studies of $Fe_{100-x}Ga_x$ and $Fe_{100-x}Al_x$ ($x=6.25-25$) alloys. The lattice sizes and atomic positions of these structures were optimized according to the energy minimization procedures guided by atomic forces. A $6\times6\times6$ Monkhorst–Pack *k*-point mesh in the Brillouin zone was used to evaluate integrals in the reciprocal space. Test calculations with a 128 atom supercell indicated that elastic constants are rather insensitive to the cell size and small changes in the distribution of minority atoms till $x=18.75$. However, results for cases with $x=25$ were strongly dependant on the local atomic arrangement so they will be discussed separately.

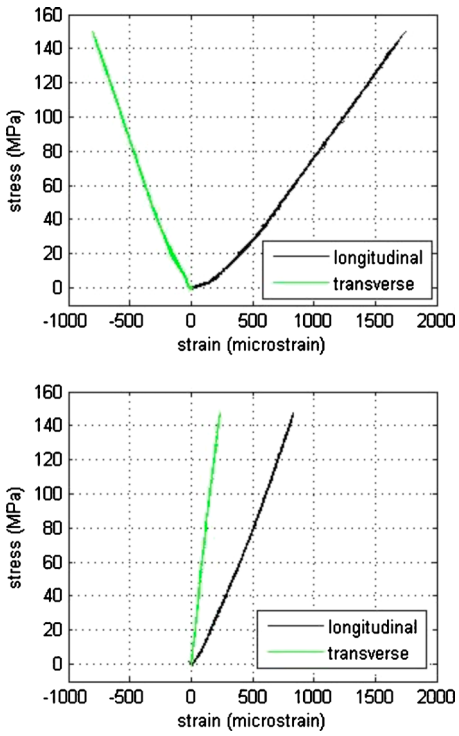

FIG. 3. (Color online) Stress-strain plots for (a) the $Fe_{88.1}Ga_{11.9}$ [100] and (b) the $Fe_{88.0}Ga_{12.0}$ [110] sample.

IV. RESULTS AND DISCUSSIONS

A. Experimental results

The data collected in the tension tests were converted into a stress versus strain plot for each specimen, as shown in Fig. 3 for $Fe_{88}Ga_{12}$ samples along the [100] and [110] axes. These data were used for the determination of Young's modulus and Poisson's ratio. Most of samples show a slight curvature in the stress-strain plot at low stress values before the dependence becomes linear. This slight curvature arises from the delta-E effect, which occurs in ferromagnetic materials due to the relationship between applied stress and local magnetization.[21,22] Elastic modulus and Poisson's ratio properties were calculated using data in the linear range, according to

$$Y = \frac{1}{n}\sum_n \frac{\sigma_n}{\varepsilon_{\text{long},n}}; \quad \text{and} \quad \nu = \frac{1}{n}\sum_n \frac{-\varepsilon_{\text{tran},n}}{\varepsilon_{\text{long},n}}, \tag{2}$$

where σ, ε, and n represent the stress, strain, and number of data points, respectively. Repeated measurements were taken to ensure the accuracy of data and provide confidence intervals for the measured results. Furthermore, we used a steel calibration sample with dimensions similar to the Galfenol specimens to check the validity of our procedure. The measured Young's modulus for steel was 217 GPa and the Poisson's ratio was 0.33, in good accordance with corresponding data in the literature, 207 GPa and 0.30.[23] Experimental results for the three compositions of $Fe_{100-x}Ga_x$ samples are presented in parentheses in Table I (under the predicted values that are discussed in Sec. IV B). The error bands represent a 95% confidence interval for measurements using different strain gauges that can be attributed to for instance, small variation in alignment of strain gauges. From these data, C' and C_{44} were calculated and the new results agree with trends in the literature. In particular, both longitudinal and transverse strains increase with the tensile stress in Fig. 3(b), which indicates the auxetic response of the $Fe_{88.0}Ga_{12.0}$ sample in the [110] direction. Although dog-bone samples of Fe–Al were not available, published values of experimentally determined elastic constants for Fe–Al (Ref. 24) are included in Table I and are used to calculate modulus and Poisson ratios.

B. Modeling results

We determined values of $\nu(110, 1\bar{1}0)$ through calculating elastic stiffness constants, by applying different strains to the lattice. Interestingly, the curves of total energies cannot be fit well with a quadratic function of ε, indicating the importance of high order contributions to elasticity of these

TABLE I. Calculated elastic properties of and ($x=6.25\sim25$) alloys accompanied by corresponding interpolated experimental data in parentheses. C_{11}, C_{12}, C_{44}, B, C', and $Y(110, 1\bar{1}0)$ are given in GPa.

	C_{11}	C_{12}	C_{44}	B	C'	$Y(110,1\bar{1}0)$	$\upsilon(110,1\bar{1}0)$
$Fe_{100-x}Ga_x$							
6.25%Ga	226	130	113	162	50	253	–0.047
12.5%Ga	206	141	116 (112±22)	163	32 (27±3)	185 (167±10)	–0.20 0.27±0.15
18.75%Ga	205	160	128 (143±60)	175	23 (22±4)	159 (158±12)	–0.379 (0.46±0.20)
25%Ga	181±23	166±30	126±12 (117±51)	174±25	8±15 (8.2±3)	73±65 (90.5±3)	–0.81±0.54 (–0.66)
$Fe_{100-x}Al_x$							
6.25%Al	239	132	120	168	53	232	–0.033
12.5%Al	188	118	110	141	35	184	–0.163
18.75%Al	202 (185)	139 (125)	128 (125)	160 (145)	32 (30)	181 (182)	–0.261 (–0.275)
25%Al	210 (171)	161 (131)	140 (132)	177 (144)	24 (20)	171 (147)	–0.389 (–0.441)

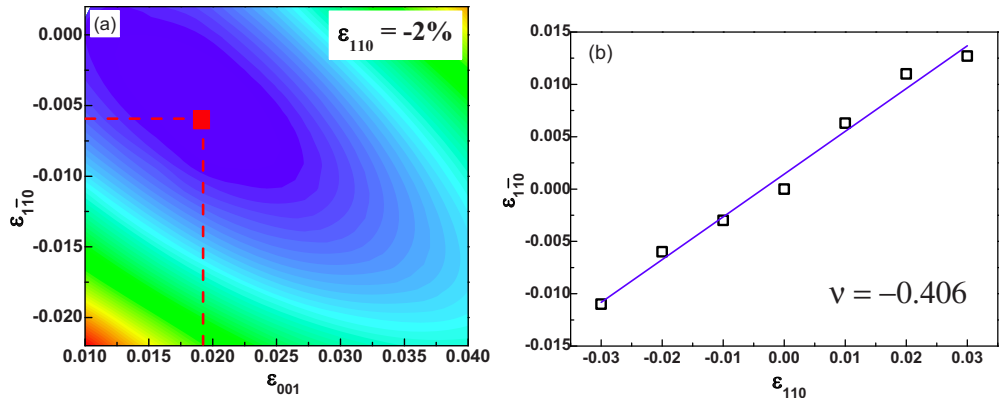

FIG. 4. (Color online) Contours of total energies versus strains along (001) and $(1\bar{1}0)$ axes for the $Fe_{12}Al_4$ alloy under a -2% artificial distortion along the (110) axis. The red square in panel (a) indicates the positions of energy minimum. Slope in panel (b) gives the Poisson's ratio $\nu(110,1\bar{1}0)$.

materials, as has been suggested by Clark *et al.*[25] Through the fitting procedure, we obtained elastic stiffness constants of different samples and used them for the determination of elastic modulus Y and Poisson ratio ν. Theoretical results are listed in Table I (above the corresponding experimental data for comparison). Overall, density functional calculations reproduced all mechanical properties very well, including the negative Poisson's ratios. Therefore, we conclude that the auxetic attributes of Galfenol and Alfenol stem from their electronic structures and, furthermore, the density functional approach used is a reliable tool for use in search new auxetic materials.

As a cross-examination, we also adopted a "direct" approach that mimics the macroscale tensile test experiments. Explicitly, we first determined the strains along $(1\bar{1}0)$ and (001) axes under the influence of external strains along the (110) direction. This is demonstrated in Fig. 4(a), where strains along $(1\bar{1}0)$ and (001) axes are obtained from the position of the minimum of the two-dimensional energy surface. The value of $\nu(110,1\bar{1}0)$ was then calculated from the slope of $\varepsilon(1\bar{1}0)/\varepsilon(110)$ as shown in Fig. 4(b). Such a direct procedure gives $\nu(110,1\bar{1}0)=-0.406$ for $Fe_{75}Al_{25}$ in the DO_3 structure. This number is very close to the corresponding value in Table I, -0.389. Therefore, one can conveniently use either the direct approach or calculations using elastic stiffness constants according to Eq. (1) for the determination of $\nu(110,1\bar{1}0)$.

It is important to point out that the calculated values of $\nu(110,1\bar{1}0)$ for $Fe_{75}Ga_{25}$ were sensitive to changes in the distribution pattern of Ga atoms in the Fe lattice. We believe this is because the homogeneous DO_3 structure is unstable to tetragonal distortion, both according to more reliable all-electron full potential linearized argument plane wave calculations and to VASP calculations with different parameters.[26] It is hence expected that Ga distribution in Fe is rather nonuniform at high concentrations, and probably is accompanied by local lattice distortions or precipitation, as reported recently by Ruffoni *et al.*[27] We incorporated the effect of random Ga distributions in $Fe_{75}Ga_{25}$ Galfenol using structures generated through molecular dynamics simulations. As a result, values of $\nu(110,1\bar{1}0)$ swing from -0.27 to -1.35. In contrast, results for $Fe_{75}Al_{25}$ are insensitive to the structural variation according to similar test calculations, which is consistent with that the DO_3 structure is stable for Alfenol.

C. Discussions

It is clear in Table I that the calculated elastic properties agree well with the experimental data. For better comparison, additional experimental data from the literature for Galfenol and Alfenol are included and plotted in Fig. 5. One can see that theory produces the trends of Poisson's ratios of both alloys in a broad range of x. No such direct quantitative comparison has been reported before for the auxetic properties of intermetallic alloys. Again, this suggests the validity

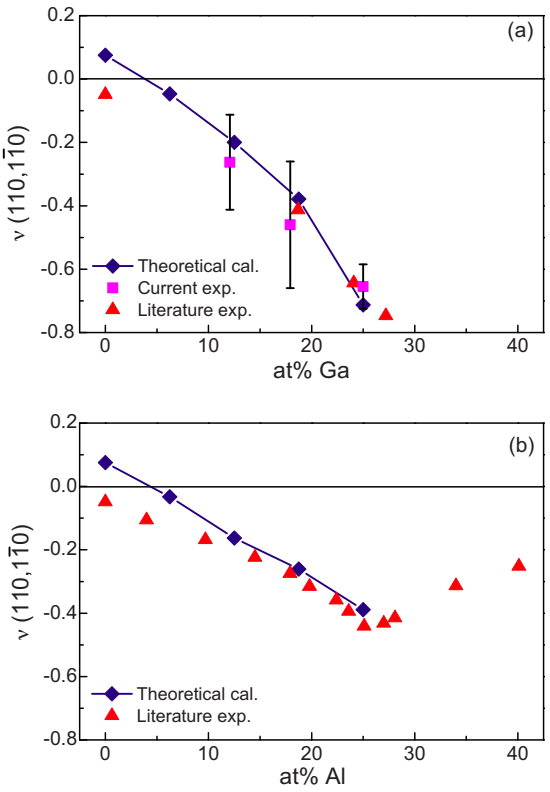

FIG. 5. (Color online) Composition dependence of Poisson's ratio of (a) Galfenol and (b) Alfenol.

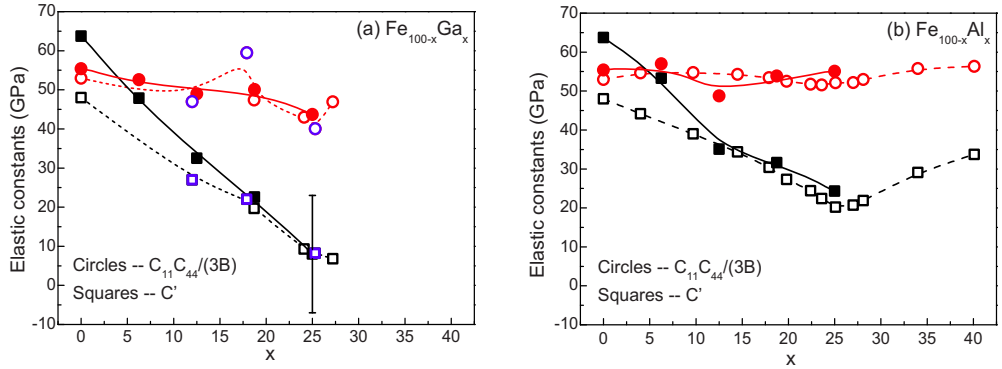

FIG. 6. (Color online) The calculated and measured values of C' and $(C_{11}C_{44})/(3B)$ for (a) Galfenol and (b) Alfenol. Open and filled symbols denote experimental and theoretical data, respectively. The blue circles and squares (dark grey) represent the new experimental data from this study. Curves are for eye guiding. The bar for C' at $x=25$ indicates the range of variation in theoretical data for structural changes.

of our theoretical approach and, moreover, the relevance of the atomic models in Fig. 2 for the determination of auxetic properties of Galfenol and Alfenol.

In Eq. (1), we found that negative Poisson's ratios occur only when C' becomes smaller than $C_{11}C_{44}/3B$. To appreciate this, we plotted the calculated results of C' and $C_{11}C_{44}/3B$ in Fig. 6. It is noteworthy that $C_{11}C_{44}/3B$ decreases very slightly with x, and hence the drop of C' is the leading factor for the change in Poisson's ratio. The correspondence between C' and $\nu(110,1\bar{1}0)$ is apparent in Figs. 5 and 6 for both Galfenol and Alfenol. The main deficiency of the present simulations is the overestimation of C' for pure Fe because of a deficiency associated with the GGA used in the calculations.

The simple correlation between $\nu(110,1\bar{1}0)$ and elastic anisotropy is important for the understanding and manipulation of auxetic properties of alloys. The drop of C' can be further connected to the tendency that Ga and Al atoms stay far apart in the Fe lattice. Furthermore, the Fe bonds toward metalloid atoms become "dangling bonds" because of the weak hybridization between Fe and Ga (or Al) states. As illustrated in Fig. 7 for the DO_3 structure, we found that pure Fe layers are separated by the adjacent Fe–Ga(Al) mixed layer along the (001) direction. This arrangement maximally reduces the number of interlayer Fe–Fe bonds, and subsequently causes the monotonic reduction in C' with the increase in x. With the removal of sticks between Fe and Ga (or Al), the network of Fe–Fe bonds in Fig. 7 is obviously weak against stress along the (001) axis. In contrast, there are three Fe layers between adjacent Ga (or Al) layers along the (111) direction. As a result, the network of Fe–Fe bonds can withstand stress along the (111) direction. Although Fig. 7 also displays hinges-type microstructure, as found in polymer foams, we don't find inverted hexagons. Therefore, we tend to attribute the auxetic properties of Galfenol and Alfenol to the drastic reduction in C' with the presence of metalloid atoms in the DO_3-type structures. Experimentally, C' of Galfenol typically decreases by a factor 2–3 from that of the bulk Fe when x is close to ~19 at. %, to ~20 GPa.[28] Further addition of Ga or Al starts developing Ga–Ga (or Al–Al) first neighbors, and the elastic anisotropy along (001) and (111) axes is weakened. This results in gradual reversal in trend and a reduction in magnitude of the negative $\nu(110,1\bar{1}0)$ with the further increase in x, as shown in Fig. 5(b) for Alfenol with x greater than ~25. Note that auxetic behavior were typically explained in terms of a "rotation of rigid units" at the molecular level, such as "rotating tetrahedra" or "rotating rectangles" for α-cristobalite.[29–31] Here we revealed that elastic anisotropy in a particular network of bonds depicted in Fig. 7 may also produce large auxetic response.

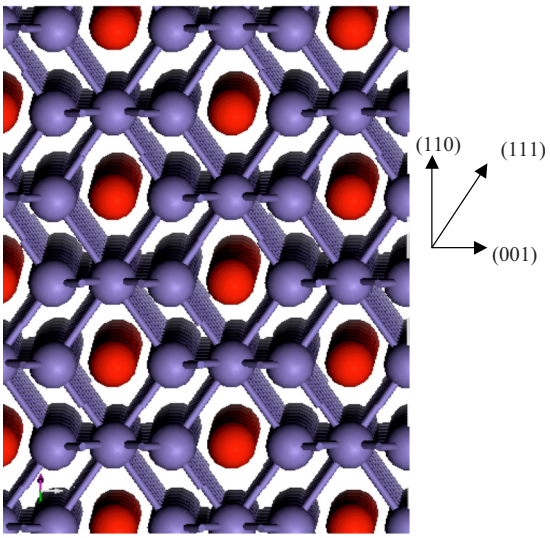

FIG. 7. (Color online) Schematic network of Fe–Fe bonds in $Fe_{75}Ga_{25}$ with DO_3 structure viewed from the $(1\bar{1}0)$ direction.

Finally, how can one further enhance the Poisson's ratio of homogeneous intermetallic alloys? It is clear from Eq. (1) that $\nu(110,1\bar{1}0)$ can only take value values between $-1(C'=0)$ and $+1(C' \gg C_{11}C_{44}/3B)$ for stable cubic materials. For the former condition, one can chose appropriate metalloid elements to further reduce C'. To this end, $Fe_{75}Ge_{25}$ might be a good candidate since our calculations showed that C' of $Fe_{75}Ge_{25}$ is smaller than 7 GPa in the DO_3 structure. From the calculated value of C_{44}, 130 GPa, we expect that $\nu(110,1\bar{1}0)$ of $Fe_{75}Ge_{25}$ can reach about -0.9. Experimental studies for single-crystal samples of $Fe_{75}Ge_{25}$ will be performed to verify this prediction.

V. CONCLUSIONS

Experimental and density functional studies were performed to attempt to explain the origin of intrinsic auxetic properties of Galfenol and Alfenol in a composition range $0<x<25\%$. Very good agreement between theory and experiment indicates the validity and usefulness of using the density functional calculations for the determination of auxetic properties. The negative Poisson's ratios were attributed to elastic anisotropy, i.e., the difference between C' and C_{44}. It can be further linked to the hinge-type microstructures after the removal of Fe bonds toward metalloid atoms. This structure is extremely soft against the [001] stress but remains tough toward the [111] stress. The mechanism responsible for the auxetic features of these iron-based alloys is thus different from what was proposed for foam and polymer auxetic materials.

Interpretation of the presented results suggests that further experimental and theoretical investigations of related alloys may lead to new and more highly auxetic structural materials. Calculations based on the theoretical approach presented predict that $Fe_{75}Ge_{25}$ will have good structural properties and Poisson ratio values that are as low in magnitude as -0.9. Experiments are needed to confirm this prediction.

ACKNOWLEDGMENTS

We thank Dr. A. E. Clark, M. Wun-Fogle, and K. B. Hathaway for stimulating discussions. Work is supported by the ONR (Grant No. N00014-08-1-0143) and NSF (Grant No. DMR-0706503). Calculations were performed on supercomputers of NAVO, ARSC, and ERDC.

[1]W. Yang, Z. M. Li, W. Shi, B. H. Xie, and M. B. Yang, J. Mater. Sci. **39**, 3269 (2004).
[2]R. S. Lakes, Science **235**, 1038 (1987).
[3]B. D. Caddock and K. E. Evans, J. Phys. D: Appl. Phys. **22**, 1877 (1989).
[4]K. E. Evans, M. A. Nkansah, I. J. Hutchinson, and S. C. Rogers, Nature (London) **353**, 124 (1991).
[5]L. Z. Chen, C. H. Liu, J. P. Wang, W. Zhang, C. H. Hu, and S. S. Fan, Appl. Phys. Lett. **94**, 253111 (2009).
[6]F. Milstein and K. Huang, Phys. Rev. B **19**, 2030 (1979).
[7]M. Jain and M. P. Verma, Indian J. Pure Appl. Phys. **28**, 178 (1990).
[8]R. H. Baughman, J. M. Shacklette, A. A. Zakhidov, and S. Stafstrom, Nature (London) **392**, 362 (1998).
[9]J. N. Grima, R. Jackson, A. Alderson, and K. E. Evans, Adv. Mater. (Weinheim, Ger.) **12**, 1912 (2000).
[10]A. Alderson and K. E. Evans, Phys. Rev. Lett. **89**, 225503 (2002); J. Phys.: Condens. Matter **21**, 025401 (2009).
[11]R. A. Kellogg, A. M. Russell, T. A. Lograsso, A. B. Flatau, A. E. Clark, and M. Wun-Fogle, Acta Mater. **52**, 5043 (2004).
[12]A. E. Clark, J. B. Restorff, M. Wun-Fogle, T. A. Lograsso, and D. L. Schlagel, IEEE Trans. Magn. **36**, 3238 (2000).
[13]A. E. Clark, K. B. Hathaway, M. Wun-Fogle, J. B. Restorff, T. A. Lograsso, V. M. Keppens, G. Petculescu, and R. A. Taylor, J. Appl. Phys. **93**, 8621 (2003).
[14]R. A. Kellogg, A. B. Flatau, A. E. Clark, M. Wun-Fogle, and T. A. Lograsso, J. Appl. Phys. **91**, 7821 (2002).
[15]A. E. Clark, J. B. Restorff, M. Wun-Fogle, K. W. Dennis, T. A. Lograsso, and R. W. McCallum, J. Appl. Phys. **97**, 10M316 (2005).
[16]Materials Preparation Center, Ames Laboratory, USDOE Basic Energy Sciences, Ames, IA, USA. See, www.mpc.ameslab.gov.
[17]H. M. Schurter, M.S. thesis, University of Maryland, 2009.
[18]Y. Wang and J. P. Perdew, Phys. Rev. B **44**, 13298 (1991).
[19]G. Kresse and J. Furthmüller, Phys. Rev. B **54**, 11169 (1996).
[20]G. Kresse and J. Joubert, Phys. Rev. B **59**, 1758 (1999).
[21]H. B. Huntington, *The Elastic Constants of Crystals* (Academic, New York, 1958), pp. 93–98.
[22]J. Atulasimha, A. B. Flatau, and R. A. Kellogg, J. Intell. Mater. Syst. Struct. **17**, 97 (2006).
[23]J. W. Dally and R. J. Bonenberger, *Design Analysis of Structural Elements* (College House, Knoxville, TN, 2003), Vol. 686.
[24]H. J. Leamy, E. D. Gibson, and F. X. Kayser, Acta Metall. **15**, 1827 (1967).
[25]A. E. Clark, J. B. Restorff, M. Wun-Fogle, D. Wu, and T. A. Lograsso, J. Appl. Phys. **103**, 07B310 (2008).
[26]We found that VASP produces comparable results as FLAPW for magnetic moments and elastic constants of Galfenol only when we set VOSKOWN = 1 in the input. In contrast, results for Alfenol are less sensitive to the choice of this parameter.
[27]M. P. Ruffoni, S. Pascarelli, R. Grössinger, R. Sato Turtelli, C. Bormio-Nunes, and R. F. Pettifer, Phys. Rev. Lett. **101**, 147202 (2008).
[28]G. Petculescu, K. B. Hathaway, T. A. Lograsso, M. Wun-Fogle, and A. E. Clark, J. Appl. Phys. **97**, 10M315 (2005).
[29]A. Yeganeh-Haeri, D. J. Weidner, and J. B. Parise, Science **257**, 650 (1992).
[30]N. R. Keskar and J. R. Chelikowsky, Nature (London) **358**, 222 (1992).
[31]J. N. Grima, R. Gatt, A. Alderson, and K. E. Evans, Mater. Sci. Eng., A **423**, 219 (2006).